Oxidovanadium(IV) sulfate catalyses light-driven C–N bond formation

Journal of Molecular Catalysis. A, Chemical xxx (xxxx) 113054

Contents lists available at ScienceDirect

Journal of Molecular Catalysis. A, Chemical

journal homepage: www.journals.elsevier.com/molecular-catalysis

Oxidovanadium(IV) sulfate catalyses light-driven C–N bond fomation

Silvia Gaspa [a], Giuseppe Sciortino [b], Andrea Porcheddu [c], Chiara Dell'Osa [a], Giuseppe Satta [a, e], Ugo Azzena [a, e], Luisa Pisano [a, e], Massimo Carraro [a, e], Daniele Sanna [d], Eugenio Garribba [f, *], Feliu Maseras [b, *], Lidia De Luca [a, *]

[a] Dipartimento di Scienze Chimiche, Fisiche Matematiche e Naturali Università di Sassari, Via Vienna 2, Sassari I-07100, Italy
[b] Institute of Chemical Research of Catalonia (ICIQ), The Barcelona Institute of Science and Technology, Avgda. Països Catalans 16, Tarragona 43007, Spain
[c] Dipartimento di Scienze Chimiche e Geologiche, Università di Cagliari Cittadella Universitaria, Monserrato I-09042, Italy
[d] Istituto CNR di Chimica Biomolecolare, Trav La Crucca 3, Sassari I-07100, Italy
[e] Consorzio Interuniversitario Reattività Chimica e Catalisi (CIRCC), Bari, Italy
[f] Dipartimento di Medicina, Chirurgia e Farmacia Università di Sassari, Viale San Pietro, Sassari I-07100, Italy

ARTICLE INFO

Keywords:
Photocatalysis
DFT Mechanism
Oxidovanadium(IV) sulfate
C–N bond formation
Aldehydes
N-chloramine

ABSTRACT

Oxidovanadium(IV) sulfate, $V^{IV}OSO_4$, is shown to catalyze efficiently the amidation of the C–H bond of aldehydes by *N*-chloramine derivatives for the selective synthesis of amides. The catalytic process is driven by visible light irradiation at room temperature, and the reaction is carried out in ethyl acetate, a green and bio-based solvent. The catalyst, as an inorganic salt of an earth-abundant transition metal, is easily available, stable and inexpensive and is superior compared to other tested transition metal salts and complexes. The proposed reaction mechanism is obtained through the use of a combination of experimental and computational techniques. EPR spectroscopy suggests an interaction of the amine with the $V^{IV}O^{2+}$ ion and the formation of V^{IV}/V^{V} and radical organic intermediates. Density functional theory (DFT) unveils a light-induced radical mechanism via an unusual $V^{IV}OCl(SO_4)$ complex. The mechanistic proposal opens perspectives for the extended application of vanadium salts toward highly desirable dechlorination processes as well as for harsh C–H activations.

1. Introduction

Photocatalysis has been one of the success stories in chemistry in the XXI century [1,2]. Photochemistry had been for a long time a well-known part of mainstream synthetic organic chemistry but relied mostly on the direct excitation of organic compounds by UV light, which limited significantly its scope [3,4]. This situation changed mainly thanks to the introduction of photosensitizers, photoactive species able to absorb photons and transfer efficiently its energy to the organic systems of interest [5]. In this way, visible-light-driven photoreactions have been shown to display a safe and more accessible alternative to traditional photochemistry, and to introduce new reactivity modes in organic synthesis.

This renaissance in photochemistry derives largely from the development of photosensitizers based on Ru(II) and Ir(III) complexes [6,7]. However, the intrinsic high cost of these noble metals, their scarceness and high toxicity profiles are clearly suboptimal. It is thus advisable to study the opportunity of replacing Ru- and Ir-based photocatalysts with more sustainable, easily accessible and cheaper metals [8–11]. Reports of earth-abundant metals (EAM_S) ed-photocatalysts have been described in recent years and include inorganic and organometallic complexes of vanadium(V) [8,9], chromium(III) [12], iron(II) [13,14], cobalt(III) [15], copper(I) [16,17], zinc(II) [18,19], zirconium(IV) [20], and tungsten(VI) [21,22], but this is clearly still an open topic. Particularly, only one V-based homogenous photocatalyst has been reported up to now; it is $V^{V}O(O^{i}Pr)_3$ which, in presence of O_2, selectively oxidizes the Cα–Cβ bond of lignin β–1 at room temperature and under visible light irradiation [23–25]. These classes of EAM_S have moreover distinct reactivity profiles, further expanding the diversity of the field [26].

Amide bonds are basic functional groups in chemistry currently exploited for natural products, functionalized materials and drugs development [27,28]. Traditional methods for the preparation of amides suffer of many drawbacks, such as the formation of byproducts, chemical waste and harsh working conditions [7,29,30].

These problems have been partially addressed by the introduction of photocatalytic procedures [31,32]. Recent examples are based on precious Ir and Ru classic photosensitizers [33,34], metallic nanocompos-

* Corresponding authors.
E-mail addresses: garribba@uniss.it (E. Garribba), fmaseras@iciq.es (F. Maseras), ldeluca@uniss.it (L. De Luca).

https://doi.org/10.1016/j.mcat.2023.113054
2468-8231/

ites [35,36], and organocatalyzed approaches [37–43]. Ball-milling [44], continuous-flow [45], Fe(III)- [46] and Rh(III)-catalysed [47] approaches for the direct aldehyde C–H amidation from aldehydes and *N*-chloroamines have been also proposed. However, there is still margin for improvement in view of industrial scale application: i) precious metal-based photosensitizers are toxic and expensive; ii) some catalysts need specific synthesis; and iii) solvents are not always green. Here we report a new class of photocatalytic system based on oxidovanadium (IV) sulfate, $V^{IV}OSO_4$, a stable, inexpensive and commercially available EAM salt. The efficiency of $V^{IV}OSO_4$ has been compared with that of other inorganic salts of first raw transition metals and metal complexes in the synthesis of amides from *N*-chloramines and aldehydes. The catalyst works in ethyl acetate, a green and bio-based solvent, and well tolerates both aromatic aldehydes and primary and secondary *N*-chloramines with diverse functional groups. Selective C–H activation remains a highly desirable goal in organic synthesis, and this work complements the range of available methods with a new photocatalytic alternative [23,25,48–52]. We also report a mechanistic study of the process by coupling spectroscopic studies and DFT calculations [53–58]. The proposed mechanism may be foundational for further exploration of the reactivity of this and related systems.

2. Experimental

2.1. General information

All reagents and solvents were as obtained by commercial source. All solvents were dried by usual methods and distilled under Argon. Column chromatography was generally performed on silica gel (pore size 60 Å, 32–63 nm particle size) and reactions were monitored by thin-layer chromatography (TLC) analysis was performed with Merck Kieselgel 60 F254 plates and visualized using UV light at 254 nm, $KMnO_4$ and 2,4-DNP staining. For irradiation with blue light OSRAM Oslon SSL 80 LDCQ7P-1U3U (blue, λ max = 455 nm, I max = 1000 mA, 1.12 W) was used. ^{1}H NMR and ^{13}C NMR spectra were measured on a Bruker Avance III 400 spectrometer (400 MHz or 100 MHz, respectively) using $CDCl_3$ solutions and TMS as an internal standard. Chemical shifts are reported in parts per million (ppm, δ) relative to internal tetramethylsilane standard (TMS, δ 0.00). The peak patterns are indicated as follows: s, singlet; d, doublet; t, triplet; m, multiplet; q, quartet; dd, doublet of doublets; br, broad. The coupling constants, J, are reported in Hertz (Hz). High resolution mass spectra HRMS (HESI-FT-ORBITRAP) were recorded on a Q-Exactive Thermo Scientific mass spectrometer. UV–Vis spectra were obtained on a Varian Cary 1E UV/VIS Spectrometer. Melting points were determined in open capillary tubes and are uncorrected.

2.2. General procedure to N-chloro-amines 2a-2o

Amine (10 mmol) was dissolved in CH_2Cl_2 (50 mL) and treated with *N*-chlorosuccinimide (11 mmol, 1.47 g) at 0 °C. After the addition, the mixture was warmed to r.t. and stirred for 2 h under Ar (the reaction was monitored by TLC until disappearance of amine). Then, the crude products were purified by flash chromatography on pad of silica gel.

2.3. General procedure to compounds 3a-3u, 4a-4n

In a round bottom flask of 25 mL, aldehyde (4 mmol) and $VOSO_4{\cdot}3H_2O$ (8.69 mg, 5% mol) were added to a solution of a *N*-chloroamine (0.8 mmol) in 1 mL AcOEt under Ar atmosphere and at room temperature. The mixture was stirred under blue led irradiation for 24 h under Ar (the reaction was monitored by TLC until disappearance of *N*—Cl-amine). Then was added NEt_3 (0.8 mmol, 0.11 mL) and the reaction mixture left to stir at room temperature for 2 h until disappearance of the intermediate acyl chloride (monitored by TLC). Then, the reaction mixture was quenched with water and extracted with AcOEt. The combined organic layers were washed three times with a solution of 5% citric acid and then three times with a solution of 5% $NaHCO_3$; the organic phase was dried over anhydrous Na_2SO_4, and the solvent was evaporated under reduced pressure. The crude products were purified by flash chromatography on silica gel.

2.4. Detection and characterization of benzoyl chloride

In a round bottom flask of 25 mL, benzaldehyde (4 mmol, 425 mg) and $VOSO_4{\cdot}3H_2O$ (8.68 mg, 5% mol) were added to a solution of a *N*-chloro-*N*-methyl-1-phenylmethanamine (0.8 mmol, 125 mg) in 1 mL AcOEt under Ar atmosphere and at room temperature. The mixture was stirred under blue led irradiation for 24 h under Ar (the reaction was monitored by TLC until disappearance of *N*—Cl-amine). The crude products were purified by flash chromatography on silica gel to provide benzoyl chloride (0.084 g, 75% yield). ^{1}H NMR (400 MHz, $CDCl_3$) δ: 8.08 (d, *J* = 7.8 Hz, 2H), 7.66 (t, *J* = 7.4 Hz, 1H), 7.48 (t, *J* = 7.6 Hz, 2H). ^{13}C NMR (100 MHz, $CDCl_3$) δ: 168.3, 135.4, 133.2, 131.4, 129.0.

2.5. Spectroscopic details

EPR spectra were recorded at room temperature with an X-band Bruker EMX spectrometer equipped with a HP 53150A microwave frequency counter. A preliminary exploration in the magnetic field range 0–8000 Gauss was carried out and, next, the spectra were recorded only in the range where absorptions are detected, in the range 2900–3900 Gauss. The microwave frequency was 9.40–9.41 GHz, microwave power was 20 mW, time constant was 81.92 ms, modulation frequency 100 kHz, modulation amplitude 0.4 mT, sweep time 335.54 s, resolution 4096 points.

UV–Vis spectra were recorded on a Varian Cary 1E spectrophotometer from 900 to 300 nm with a scan rate of a 0.5 nm/s.

2.6. Computational details

Mechanistic analysis has been performed at DFT level of theory using Gaussian16 software [59]. All structures were optimized in DCM modelled with the SMD continuum model [60] using the B3LYP functional [61] combined with the Grimme's D3 correction for dispersion [62]. Basis set BS1 was used for the optimizations. BS1 includes the 6–31G(d,p) basis set for the main group elements [63], and the scalar relativistic Stuttgart-Dresden SDD pseudopotential and its associated double-ζ basis set [64], complemented with a set of *f* polarization functions [65] for the vanadium atom. Frequency calculations were carried out for all the optimized geometries in order to characterize the stationary points as either minima or transition states. It was confirmed that transition states connect with the corresponding intermediates by usual intrinsic reaction coordinate (IRC) calculations and subsequent optimization to minima. Final Gibbs energies were obtained by adding the thermal and entropic corrections obtained with BS1 to the potential energies obtained with single point calculations using an extended basis set (BS2). BS2 consists in the triple-ζ def2-TZVP basis set for the main group elements and quadruple-ζ def2-QZVP basis set for V [66,67]. A correction of 1.9 kcal·mol^{-1} was applied to all Gibbs values to change the standard state from the gas phase (1 atm) to solution (1 M) at 298.15 K [68]. The electronic transitions of the intermediate II and III were computed on the optimized geometry for the ground electronic state at TD-DFT level of theory, with SMD for DCM. The CAM-B3LYP [61] functional combined with BS2 basis-set was used. The molecular orbitals (MOs) involved in the transitions were simulated performing a Mulliken population analysis (MPA) with Gaussian 16 at the same level of theory used for the TD-DFT calculations and identified via the AOMix package (vers. 6.52) [69].

Minimum Energy Crossing Points (MECPs) between potential energy surfaces of different spin have been computed using the program developed by Harvey and co-workers [70]. To confirm that the MECPs relate the two potential energy surfaces, the MECP structures were optimized in the different spin states involved in the crossing. Gibbs energies of MECPs were estimated for both spin states by adding the enthalpic and entropic correction computed at BS1 level to the single point energy computed at BS2 level. The final energy is the average of the values computed for both spin states.

Nudged Elastic Band (NEB) calculation has been carried out using ORCA 4.0.1 at DFT B3LYP-D3 theory level generating a total of six images connecting intermediates VIII and IX [71].

Orbital localization of canonical Density Functional Theory orbitals [72] was performed with the CP2K code (www.cp2k.org) using the PBE exchange-correlation functional [73]. The Quickstep algorithm was applied to solve the electronic structure problem [74], employing a double- ζ plus polarization (DZVP) basis set to represent the valence orbitals and plane waves for the electron density (300 Ry cutoff). Goedecker-Teter-Hutter (GTH) type pseudopotentials were used for valence-core interactions [75,76]. Models were treated as isolated in a cubic box of 30 Å edge.

3. Results and discussion

In relation to our interest in the synthesis of amides [77,78], we evaluated the possibility to directly use EAMs-based salts as photocatalysts for selective amidation of aldehydes.

The investigation started reacting benzaldehyde 1a with *N*-chloro-*N*-methyl-1-phenylmethanamine 2a as the model substrates, using an array of V-, Mn-, Fe-, Co-, Ni- and Cu-based EAMs salts and complexes under light irradiation by blue (455 nm) or green (535 nm) LED_s (Table 1). In the first reaction, benzaldehyde (Table 1, 1a, 4 mmol), *N*-chloro-*N*-methyl-1-phenylmethanamine (Table 1, 2a, 0.8 mmol) and $V^{IV}OSO_4$ (Table 1, 5 mol%) in 1 mL of DCM were irradiated for 24 h with blue LED_S. Then Et_3N (0.8 mmol) was added, affording the product 3a in 68%. For comparison, a stable $V^{IV}O$ complex, $V^{IV}O(acac)_2$, where acac is acetylacetonato ligand, and a vanadate(V) salt, $NH_4V^{V}O_3$, have been tested, yielding 3a in 7% and 44%, respectively (Table 1, entries 2 and 3). With the iron salts $Fe^{II}Cl_2$ and $Fe^{III}Cl_3$, the product 3a was formed in 34 and 30% yield, respectively, under blue LED irradiation (Table 1, entries 4 and 5). $Ni^{II}SO_4$ has given similar results, affording the desired product in 25% yield (Table 1, entry 6). Copper salts such as $Cu^{I}Cl$ and $Cu^{II}(OAc)_2$ were tested furnishing the product 3a in 37% and 10%, respectively (Table 1, entries 7 and 8). Other metal salts like $Mn^{II}Cl_2$, $Co^{II}Cl_2$ and $V^{III}Cl_3$ with maximum absorbance around 535 nm (green led) did not lead to the product (Table 1, entries 9, 10 and 11). Comparing all the systems, $V^{IV}OSO_4$ afforded the product 3a with the most promising yield of the set achieving 68% (Table 1, entry 1). With this result in hand, a solvent screening has been performed. In acetonitrile (CH_3CN) and cyclopentyl methyl ether (CPME), the yield was not enhanced (Table 1, entries 12 and 13). Concerning the molar ratio of 1a and 2a, it was found that an excess of 5 equiv. of 1a was a good compromise between the reactive loading and yield of the reaction (see Table S1). However, at the end of the reaction (Table 1, entry 14), 60% of unreacted aldehyde was recovered. To our delight, when ethyl acetate (AcOEt) was used as a solvent, the yield increased up to 80% (Table 1, entry 14). It is to highlight that AcOEt, being biodegradable and not bioaccumulable is a highly recommended solvent by Sanofi's solvent selection guide [79], and also included in the greener solvent GSK's list [80]. In contrast, when the reaction with $V^{IV}OSO_4$ as a photocatalyst was performed in dark and under green LEDs irradiation (Table 1, entries 15 and 16), no products were obtained. This finding confirms a blue LEDs light-activation process. Finally, $Ru^{II}(bpy)_3Cl_2$, a classical photocatalyst, was also tested for comparison, but no products have been detected (Table 1, entry 17).

Table 1
Screening for the selective amidation of 1a and 2a.

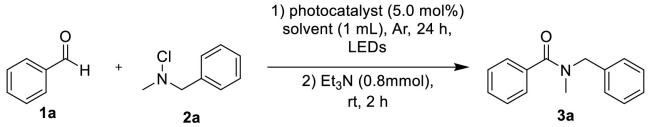

Entry[a]	Catalyst	λ (nm)	Solv.	Yield[b]
1	$V^{IV}OSO_4$	455	DCM	68
2	$V^{IV}O(acac)_2$	455	DCM	7
3	$NH_4V^{V}O_3$	455	DCM	44
4	$Fe^{II}Cl_2$	455	DCM	34
5	$Fe^{III}Cl_3$	455	DCM	30
6	$Ni^{II}SO_4$	455	DCM	25
7	$Cu^{I}Cl$	455	DCM	37
8	$Cu^{II}(OAc)_2$	455	DCM	10
9[c]	$Mn^{II}Cl_2$	535	DCM	0
10[c]	$Co^{II}Cl_2$	535	DCM	0
11[c]	$V^{III}Cl_3{\cdot}3THF$	535	DCM	0
12	$V^{IV}OSO_4$	455	CH_3CN	43
13	$V^{IV}OSO_4$	455	CPME	14
14	$V^{IV}OSO_4$	455	AcOEt	80
15	$V^{IV}OSO_4$	dark	AcOEt	0
16[c]	$V^{IV}OSO_4$	535	AcOEt	0
17	$Ru^{II}(bpy)_3Cl_2$	455	DCM	0

[a] Reaction conditions: *N*-chloro-amine (0.8 mmol), aldehyde (4 mmol), solvent (1 mL), photocatalyst (5%), blue LED_S (455 nm), 24 h. Then Et_3N (0.8 mol) for 2 h. [b]Isolated% yields. [c]The reaction mixture was irradiated for 24 h with green LED_S (535 nm).

This observation suggests an inner-sphere reaction mechanism, likely a hallmark of photocatalytic cycles involving first-row transition metal complexes, as highlighted in several reviews on photoredox catalysis with EAMs [5]. Using the optimized conditions (Table 1, entry 14), the reaction scope has been investigated. Firstly, the reactivity of an array of commercially available aldehydes has been tested. In particular, diverse functional groups on aromatic rings, both electro-donating and electron-withdrawing, were examined. Neither the electronic properties nor the steric effects of substituents on the aromatic ring of aldehydes have showed significant effect on the reaction and products yield. Strong electron-donating groups as OMe in *meta*- and *para*-positions (Scheme 1, 3b and 3c) showed satisfying results. Substituents in *ortho* positions, which are sterically hindered, as *ortho*-methoxybenzaldehyde and *ortho*-methylbenzaldehyde, were well tolerated and converted into the corresponding amide (Scheme 1, 3d and 3g). Aromatic aldehydes with moderate electron-donating substituent as methyl in *ortho, meta* or *para* positions (Scheme 1, 3e, 3f, 3g) and *tert*-butyl (Scheme 1, 3i) were converted into the corresponding amides providing satisfactory yields. When the aromatic ring was replaced by biphenyl or by hindered naphthyl groups, the corresponding amides were obtained with 49% and 65% yields, respectively (Scheme 1, 3j and 3k).

Benzaldehydes with halide substituents, as fluorine, chlorine and bromine, were subjected to the optimized reaction conditions furnishing the corresponding amides, which could be further manipulated by traditional cross-coupling reactions (Scheme 1, 3l, 3m and 3n). Benzaldehydes with moderate electron-withdrawing groups as ketone and ester gave good results too (Scheme 1, 3o and 3p). Strong electro-withdrawing groups as CN and CF_3 (Scheme 1, 3q and 3r) were well tolerated affording the desired amides in good results. To prove the synthetic utility of the procedure, thiophene-2-carbaldehyde was subjected

Table 2
Computed S^2 and Mulliken spin population for selected atoms of the open-shell intermediates and TSs [a].

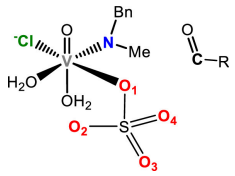

Species	S^2	V	O_1	O_2	O_3	O_4	N	C
Cat	0.76	1.12	0.02	0.00	0.00	0.00	–	–
I	0.76	1.14	0.01	0.01	0.00	0.00	0.02	–
II	0.76	1.13	0.02	0.00	0.00	0.00	0.02	–
TS_{II-III}	0.77	0.70	0.01	0.00	0.00	0.00	0.17	–
III	0.76	0.08	0.03	0.01	0.00	0.00	0.81	–
IV	3.77	1.09	0.02	0.50	0.52	0.06	0.87	–
V	3.77	1.09	0.01	0.03	0.00	0.00	0.87	0.58
VI	3.77	1.09	0.00	0.00	0.00	0.00	0.87	0.71
TS_{VI-VII}	3.77	1.08	0.01	0.00	0.00	0.00	0.87	0.71
VII	3.77	1.08	0.01	0.00	0.00	0.00	0.87	0.71
VIII	0.75	0.00	0.00	0.00	0.00	0.00	0.00	0.71
IX	0.76	1.06	0.01	0.00	0.00	0.00	0.00	0.00
TS_{IX-X}	0.76	1.13	0.01	0.00	0.00	0.00	0.05	0.00
X	0.76	1.14	0.01	0.00	0.00	0.00	0.06	0.00
XI	0.76	1.11	0.01	0.00	0.00	0.00	0.04	–
TSX_{I-XII}	0.76	1.01	0.00	0.00	0.00	0.00	0.01	–
XII	0.76	1.13	0.01	0.00	0.01	0.00	0.02	–
XIII	0.76	1.15	0.01	0.00	0.00	0.00	0.02	

[a] B3LYP-D3/BS2 in DCM continuum model.

to the optimized reaction conditions, giving the desired heteroaryl amide (Scheme 1, 3*s*). Then, aliphatic aldehydes were tested but no products were obtained (Scheme 1, 3t and 3u).

To investigate the scope of the method, the reaction was tested with an array of *N*-chloro primary and secondary amines showing a good tolerance. Primary *N*-benzyl amine provided the corresponding amide in very good yield (Scheme 2, 4a). *N*-chloro *ortho*- and *para*-methoxy benzyl amines were converted into respectively *N*-(2-methoxybenzyl) benzamide and *N*-(4-methoxybenzyl)benzamide in 59% and 76% yields (Scheme 2, 4b and 4c). In addition, *N*-chloro benzyl amines with alkyl and phenyl substituents furnish the corresponding amides (Scheme 2, 4d and 4e).

Benzyl amine with halide substituent as chlorine was employed to obtain *N*-(4-chlorobenzyl) benzamide (Scheme 2, 4f) which can be additionally transformed by cross-coupling reactions. Strong electro-withdrawing groups as CF_3 (Scheme 2, 4g) is well tolerated affording the desired amide in good yield. Primary *N*-chloro alkyl amines as heptyl and 2-phenylethane were reacted furnishing the corresponding amides (Scheme 2, 4h, and 4i). Secondary aliphatic amines both acyclic as dibenzyl amine and dibutylamine and cyclic as piperidine, 4-methylpiperidine and morpholine showed a good tolerance providing the corresponding amides (Scheme 2, 4j, 4k, 4l, 4m and 4n) in satisfactory yields.

The novelty of the photocatalyzed process led us to perform an integrated experimental/computational mechanistic analysis. A series of EPR spectra (instrumental details in the Supporting Information, SI) of the reaction mixture with 1a and 2a in AcOEt were collected in dark and under blue LED_s irradiation at different times (Fig. 1). Initially, no EPR signals are observed (trace a of Fig. 1) and only after 6 h the eight resonances due to the interaction of the unpaired electron on V^{IV} with the ^{51}V nucleus ($I = 7/2$) appear (trace b) [81]. The intensity of the spectral signals increases with time; after 14 h a well-resolved isotropic spectrum is obtained with spin Hamiltonian EPR parameters $g_{iso} = 1.975$ and $A_{iso} = 97.7 \times 10^{-4}$ cm^{-1} (trace c). Based on the 'additivity relationship', the empirical rule that assigns a contribution to each donor

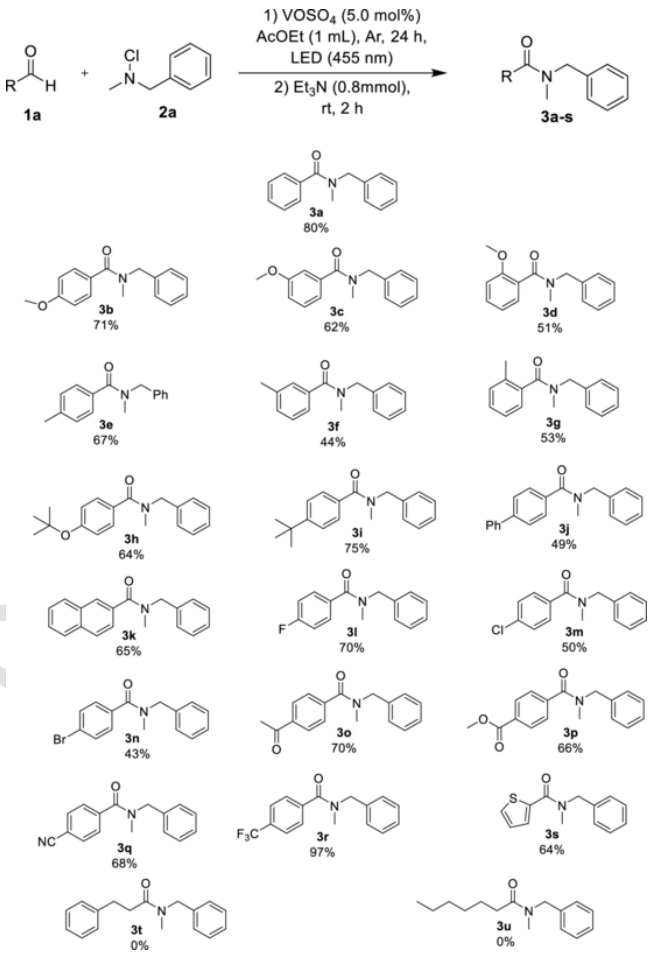

Scheme 1. Investigation of the aldehyde scope of the reaction.

in the equatorial plane and allows to estimate A_{iso}within approximately $\pm 3 \times 10^{-4}$ cm^{-1} from the experiment [82,83], this value is compatible with the binding of an amine-N to vanadium (intermediate I in the proposed mechanism, *vide infra* in Scheme 3).

Unexpectedly, the spectrum recorded after 13 h on the reaction mixture held in dark for 1 h shows that the signals of V^{IV} significantly weaken (trace d). The decrease of the EPR intensity indicates an oxidation, at least partial, to V^{V} in the absence of irradiation (intermediate III in the mechanism). In the traces a-b of Fig. 2, the spectrum of the reaction mixture blocked after 13 h and not irradiated for 1 h was again reported and compared with the same spectrum amplified 10 tens. Besides the residual signals of the V^{IV} intermediate with the amine binding (cfr. with trace c of Fig. 1), other resonances denoted with the asterisks suggest the formation of radical species and/or additional $V^{IV}O$ complexes (these could be attributed to the intermediate III). Unlikely, the isolation of such intermediates was not possible due to their low half-life. Only when the mixture is irradiated again by blue LED_s, the intensity of the resonances of $V^{IV}O$ species with the amine-N coordinated to V increases again (traces c-d), giving the final $V^{IV}O$ species of the process (Scheme S1 in the SI).

Globally, these results are in agreement with the computationally proposed mechanism showing quite low barriers and a fast evolution of the reaction after the light excitation (*vide infra*).

These results indicate that the wavelength of the blue LED_s would cause the conversion of V^{V} to V^{IV}. To confirm this assumption, the electronic absorption spectrum of the reaction mixture was recorded (Fig. 3). It can be noted that the light absorption is negligible at 535 nm (green LED_s) and increases considerably at 455 (blue LED_s), accounting for the significant difference in the yield of the reactions observed in the

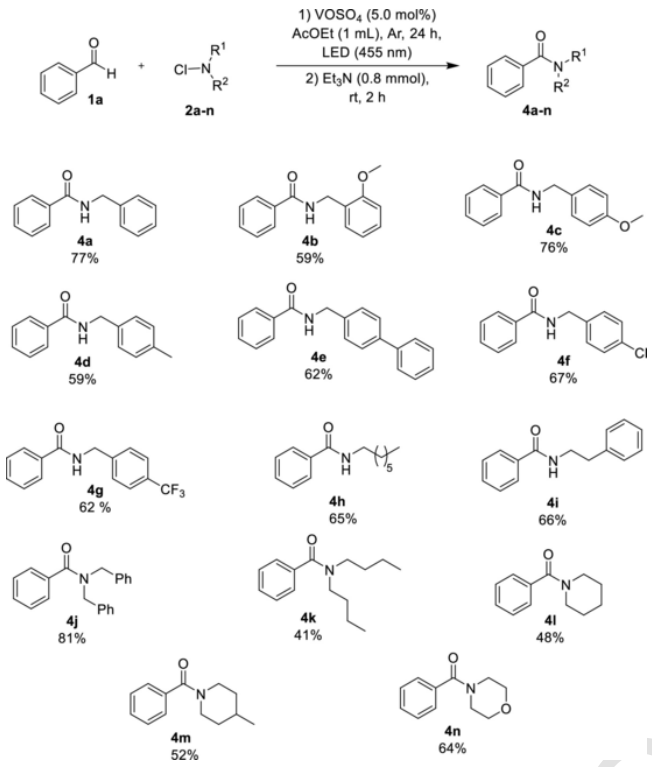

Scheme 2. Investigation of the amine scope of the reaction.

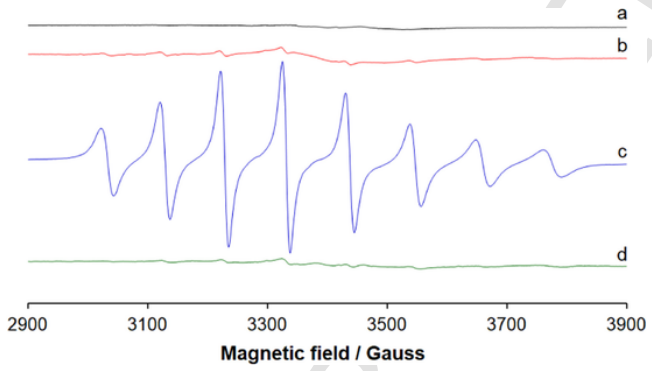

Fig. 1. EPR spectra recorded as a function of the time in the reaction mixture with 1a and 2a. (a) t = 0 h; (b) 6 h; (c) 14 h; (d) reaction blocked after 13 h and not irradiated for 1 h. The spectra were presented with the same instrumental gain.

two cases. The weak absorptions between 600 and 750 nm (trace b of Fig. 3) can be attributed to the $V^{IV}O$ intermediate(s). Finally, it must be mentioned that, among the intermediates of the reaction, an acyl chloride was also isolated and characterized through ^{1}H NMR and ^{13}C NMR [84].

The mechanistic observations from experiment were complemented by a set of DFT calculations (B3LYP-D3 in DCM continuum model, full computational details in the SI). This led to the mechanism proposed in Schemes 3 and 4. The catalytic cycle starts with the N-coordination of the chloroamine 2a to $[V^{IV}O(SO_4)(H_2O)_3]$ giving rise to the 6-coordinated intermediate I. This corresponds to the species observed by EPR spectroscopy (Figure 1, trace c, and Fig. 2, trace d). The time-dependent DFT (TD-DFT) analysis of the vertical transitions from I yielded only ligand based transitions, thus not compatible with the reported photo-redox process (see the SI for further details). Therefore, we moved to the following intermediate. Through oxidative addition (OA) the N–Cl bond is broken, entailing the formation of a V^{V} chloride complex, III, with a radical nitrogen coordinated to the metal. This oxidation process can account for the weakening of the EPR signal observed in a non-irradiated solution (Fig. 1, trace d).

In II a coordinated H_2O molecule moves to the second coordination sphere of the complex leaving a free coordination site for OA to take place (see Fig. S1 of the Supporting Information for further details). The N–Cl bond cleavage in $TS_{II\text{-}III}$ was analyzed in detail by computing the centroids of the localized molecular orbitals (CLMOs) along the reaction coordinate [72]. This demonstrates the heterolytic nature of this step, in which a concomitant single-electron transfer (SET) occurs from V^{IV} to the coordinated aminic nitrogen forming $[V^{V}OCl(SO_4)(H_2O)_2(N\text{-}2a)]$ at 1.6 kcal·mol^{-1} (Fig. 4).

The OA addition is the highest computed energy barrier of the whole cycle, 23.0 kcal·mol^{-1} (from −4.2 to 18.8 kcal mol^{-1}). We postulate that the photoactive species is intermediate III, resulting from the oxidative addition. TD-DFT indicates absorption of blue LED_s irradiation which produces a high energy excited state that could decay in a V^{IV} intermediate IV, in which an electron from the coordinated O-sulfate is transferred to the metal. The vertical excitation falling from 495 up to 377 nm were analyzed in terms of molecular orbitals (MOs) and their atomic orbitals (AOs) composition. A ligand-to-metal charge transfer (LMCT) process were clearly identified involving SO_4-π → V-$d_{x^2-y^2}$ and L'-π / SO_4-π → V-$d_{x^2-y^2}$ transitions, where L' is the coordinated amine moiety (see Table S1). The LMCT character of the transition is further supported by the approximate value 427.5 nm obtained as rough difference between ligand oxidation ($SO_4^{-\bullet}/SO_4^{2-}$) and metal reduction ($V^{V}O^{2+}/V^{IV}O^{2+}$) potentials using the literature experimental data [85–87]. This step is in agreement with the increase of the EPR intensity after the irradiation of the reaction mixture kept in dark (Fig. 1, trace e).

In the resulting intermediate IV, the original +IV oxidation state of vanadium is restored giving rise to a quartet spin state (S = 3/2) where the three unpaired electrons are localized in different centers: one on the metal, one on the coordinated N-imino and the third one on the O-sulfate (Fig. 5 and Table 2). This unusual quartet species should be extremely reactive and probably, for this reason, it is not revealed by EPR spectroscopy.

It is so reactive that is able to activate the aldehydic C–H bond in a barrierless process forming acyl radical and hydrogen sulfate. From intermediate IV the activation of the C–H bond by the N-radical was also evaluated obtaining an energy barrier of 17.1 kcal·mol^{-1}, much higher than that of the acitivation by the O-sulfate, thus confirming the proposed activation. The formation of the radical species is also suggested by EPR (Fig. 2). In the most favoured pathway the C–H aldehyde bond of IV is homolitically broken by the O-radical in a barrierless process giving rise intermediate V at 9.8 kcal·mol^{-1}. This species presents the coordinated hydrogen sulfate and the acyl radical in the second coordination sphere of the complex that can easily moves toward the chloride giving rise the almost isoenergetic intermediate VI. Through $TS_{VI\text{-}VII}$ (4.4 kcal·mol^{-1}) describing the rotation of the S–O bond, intermediate VII is formed at 8.1 kcal·mol^{-1}. In intermediate VIII (S = 1/2), falling at 5.3 kcal·mol^{-1}, a $V = N$ nitrene bond is formed entailing the oxidation of the metal centre. The different spin state potential energy surfaces of intermediate VII and are connected by minimum energy crossing point (MECP) of 5.7 kcal·mol^{-1}. The new acyl radical can easily move in the second coordination sphere approaching the chloride and spontaneously forms the new C–Cl with a concomitant single-electron transfer (SET) from the chlorine to V(V) that returns in its initial oxidation state +IV in intermediate IX at −6.6 kcal·mol^{-1} (Scheme 4). For the sake of the completeness, we estimated the energy associated with this movement through NEB calculation obtaining a potential energy barrier of 5.9 kcal·mol^{-1}. The presence of V^{IV} intermediates different from I is also consistent with the results of EPR spectroscopy (Fig. 2, traces b and c).

Intermediate IX contains the coordinated acyl chloride which can be easily dissociated through $TS_{IX\text{-}X}$, with a barrier of 1.0 kcal mol^{-1}. Inter-

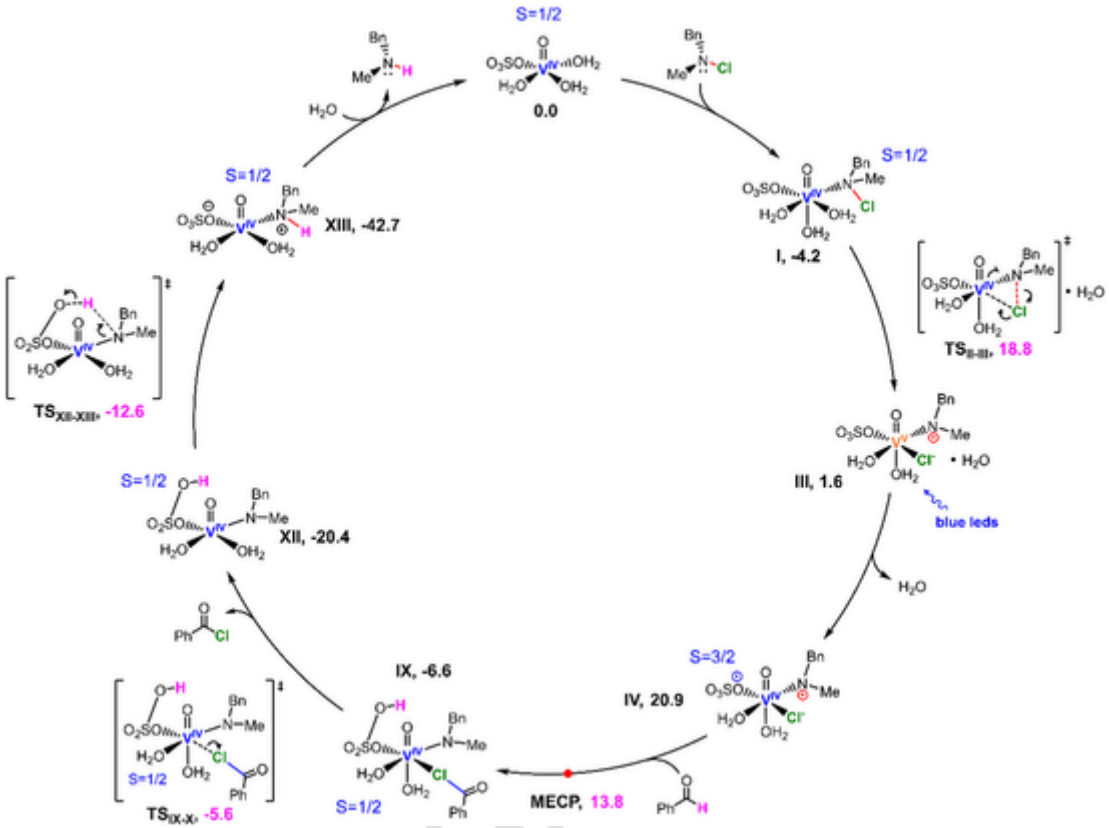

Scheme 3. Simplified DFT mechanism (energies in kcal mol^{-1}) for the $V^{IV}OSO_4$ photocatalyzed cross-coupling of benzaldehyde 1a and *N*-chloro-*N*-methyl-1-phenylmethanamine 2a to form benzoyl chloride and dimethylamine. Transition state energies are shown in purple, spin states in blue. Steps from IV to IX are depicted in Scheme 4.

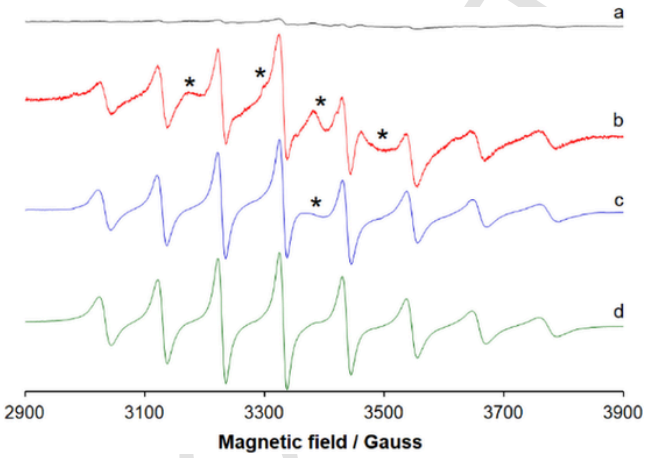

Fig. 2. EPR spectra recorded on the reaction mixture with 1a and 2a. (a) Reaction blocked after 13 h and not irradiated for 1 h; (b) same spectrum of the trace a amplified 10 times; (c) reaction blocked after 13 h, not irradiated for 1 h and irradiated again for 2 min; (d) reaction blocked after 13 h, not irradiated for 1 h and irradiated again for 5 min. The spectra were presented with the same instrumental gain, except that in the trace b. The asterisks denote radical species and/or other $V^{IV}O$ intermediates other than the one with the amine-N coordination expected on the basis of the reaction mechanism in Scheme 3.

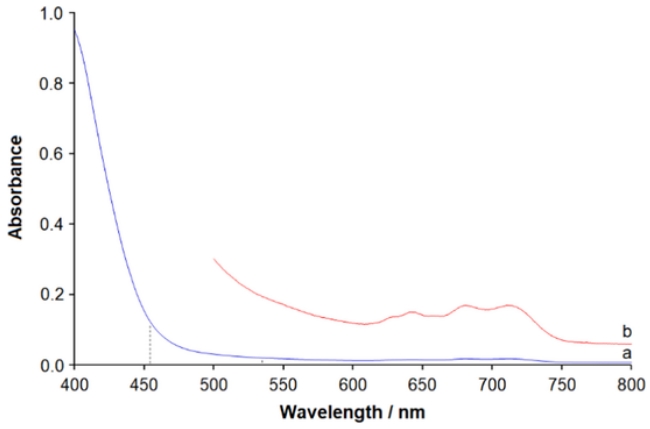

Fig. 3. Electronic absorption spectrum on the reaction mixture with 1a and 2a, irradiated for 14 h. (a) Spectral signal; (b) signal amplified 10 times. The molar amount of $V^{IV}OSO_4$ is 4.0 μmol in 1 mL of solution for a theoretical concentration of 0.004 M. The calculation of the absorption molar coefficient ε is not possible because the amount of vanadium dissolved in solution cannot be quantified. The wavelength corresponding to blue (455 nm) and green (535 nm) LED_s are shown with the dotted line.

mediate XII evolves in turn through proton migration from hydrogen sulfate to nitrogen *via* $TS_{XII-XIII}$, with a barrier of 8.2 kcal mol^{-1}. The amine is finally released and replaced by a water molecule to return to I.

The catalytic cycle results thus in the formation of acyl chloride and amide molecules, which then form a new amidic C–N bond through the well-known off-cycle nucleophilic addition-elimination reaction between the acyl chloride and the amine [88].

The proposed cycle accounts for both the low amidation yield obtained with $V^{IV}O(acac)_2$ (entry 2 of Table 1), and for the observed inertness of the aliphatic aldehydes (3t and 3 u in Scheme 1). On one hand $V^{IV}O(acac)_2$ is a species with relative low tendency of the acac ligand

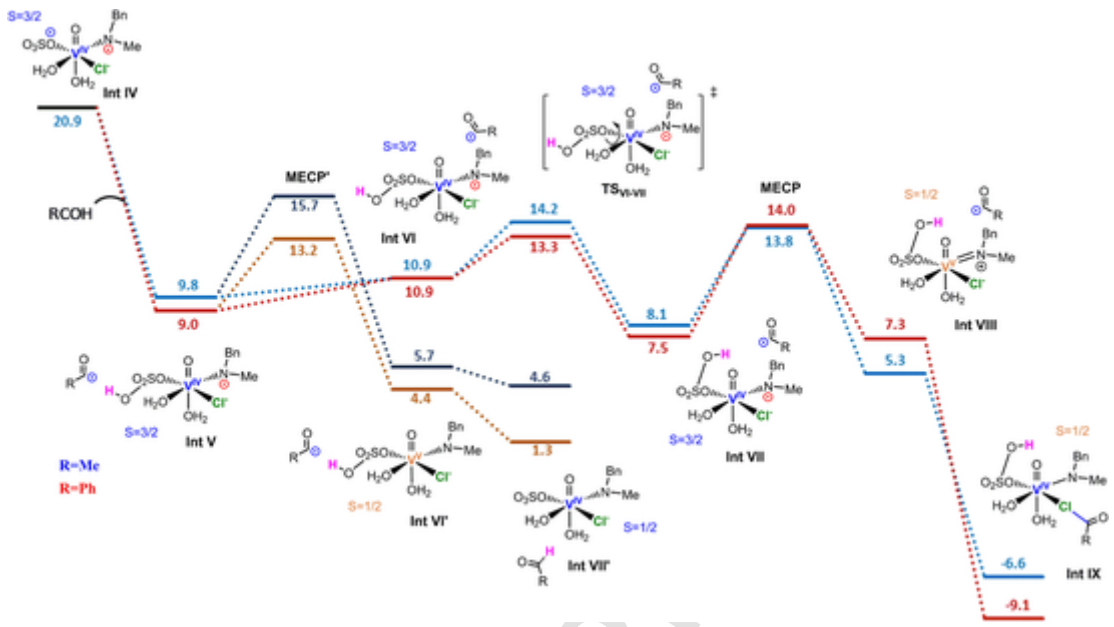

Scheme 4. DFT computed energy profile (B3LYP-D3 in DCM) for the competition between the energy profiles leading to the products (Int V to Int IX) through MECP, and to the regeneration of the reagents (Int V to Int VII') through MECP'. Light blue and red lines correspond to the main reaction for benzaldehyde and acetaldehyde, respectively. Dark blue and orange lines correspond to the deactivation paths. Spin state of the system is also specified.

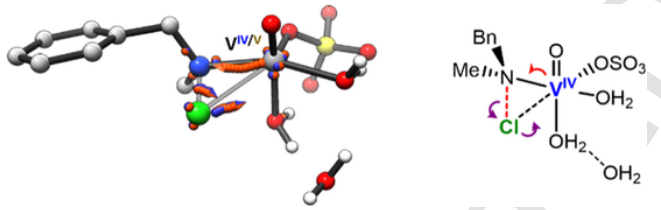

Fig. 4. Superposition over the reactant structures of the localized α and β orbital centroids (orange and blue dots, respectively) along the IRC for the oxidative-addition process. The corresponding arrow-pushing scheme is also depicted.

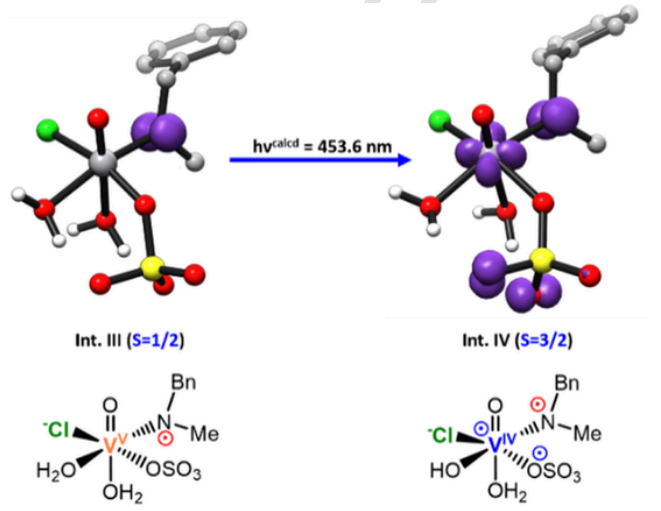

Fig. 5. Total (α–β) spin density (isovalue: 0.03) plot over intermediate III (doublet state) and intermediate IV after irradiation by blue LED_s (quartet state), see Table 2 for spin population along the reaction coordinate. The wavelength computed by TD-DFT (CAM-B3LYP) for this transition is also reported. On the bottom the corresponding structures are depicted.

toward substitution reactions and, for this reason, it is inefficient towards the OA of the *N*-chloramine; moreover, it cannot bind SO_4^{2-} due to the absence of available equatorial coordination sites around vanadium leading to less catalytically efficient excitations.

On the other, the inertness of the aliphatic aldehydes comes from an alternative evolution of V in which an additional MECP (MECP') leads to the relaxation of the excited V^{IV} complex ($S = 3/2$) that evolves toward the regeneration of the initial V^{IV} catalyst ($S = 1/2$) and the aldehyde reagent through a barrierless hydrogen abstraction. This route is favored for the aliphatic aldehyde (MECP' more stable than MECP for acetaldehyde) and disfavored for the aromatic aldehydes (MECP more stable than MECP' for benzaldehyde) (Scheme 4, orange and dark blue pathways).

Two important features of the catalytic cycle are the presence of the photochemically active intermediate III, containing V^{V}, and of intermediate V, resulting from its photoexcitation, involving spin delocalization over the sulfate ligand.

4. Conclusions

The oxidovanadium(IV) salt $V^{IV}OSO_4$ has been shown to be a new photocatalyst with application as a light-driven alternative pathway to conventional C–H aldehyde amidation leading to the selective production of amides. The advantages of $V^{IV}OSO_4$ compared to other EAM_S based-photocatalysts are: it is a common inorganic salt, is stable and inexpensive, and does not need to be synthesized. The catalyst tolerates well both aromatic aldehydes and primary and secondary *N*-chloramines with various functional groups. Spectroscopic studies, coupled with DFT calculations, suggest an inner-sphere mechanism starting with the coordination of the amine that undergoes to oxidative addition forming a photocalitically active V^{V} chloride intermediate. This V^{V} species can absorb blue LED_s irradiation to yield a highly reactive V^{IV} intermediate in the quartet spin state able to spontaneously activate aldehyde C–H bonds. The current study paves the way for general application of the $V^{IV}OSO_4$ catalyst with one unpaired electron toward highly desirable dechlorination processes as well for harsh C–H activations.

The Supporting Information (SI) is available free of charge on the ACS Publications website. Characterized compounds, extended descrip-

tion of the computational results and Cartesian coordinates of all the optimized structures (PDF). A collection set of computational data is available in the ioChem-BD repository [89].

CRediT authorship contribution statement

Silvia Gaspa : Investigation, Formal analysis, Writing – review & editing. **Giuseppe Sciortino :** Investigation, Formal analysis, Writing – review & editing. **Andrea Porcheddu :** Writing – review & editing. **Chiara Dell'Osa :** Investigation, Data curation. **Giuseppe Satta :** Investigation, Data curation. **Ugo Azzena :** Writing – review & editing. **Luisa Pisano :** Writing – review & editing. **Massimo Carraro :** Writing – review & editing. **Daniele Sanna :** Investigation, Data curation. **Eugenio Garribba :** Conceptualization, Writing – original draft, Supervision. **Feliu Maseras :** Conceptualization, Writing – original draft, Supervision. **Lidia De Luca :** Conceptualization, Writing – original draft, Supervision.

Declaration of Competing Interest

The authors declare that they have no known competing financial interests or personal relationships that could have appeared to influence the work reported in this paper.

Data availability

Data will be made available on request.

Acknowledgments

This work was financially supported by the Regione Autonoma della Sardegna within the project "Green Chemistry in Drug Discovery": sintesi sostenibili di nuovi inibitori di telomerase" (RASSR81788-Bando Invito a presentare progetti di ricercar di base-Annualità 2017), Università di Sassari within "Finanziamento straordinario una tantum per la ricerca 2019″, (project FAR2019DELUCA), Università di Sassari within "Finanziamento straordinario una tantum per la ricerca 2020″, Fondazione di Sardegna (project FdS2017Garribba), CERCA Programme/Generalitat de Catalunya, and Spanish MCIN/AEI (PID2020–112825RB-I00 and CEX2019–000925-S). GS thanks Spanish MCIN' Juan de la Cierva program, FJC2019–039135-I.

Supplementary materials

Supplementary material associated with this article can be found, in the online version, at doi:10.1016/j.mcat.2023.113054.

References

[1] C.R. Stephenson, T.P. Yoon, D.W. MacMillan, Visible Light Photocatalysis in Organic Chemistry, John Wiley & Sons, 2018.
[2] S.C.F. Sestini, Gazz. Chim. Ital. III (1873) 241–251.
[3] G. Ciamician, P. Silber, C. Lichtwirkungen, Ber. Dtsch. Chem. Ges. 34 (1901) 1530–1543, https://doi.org/10.1002/cber.19010340232.
[4] G. Ciamician, P. Silber, Ueber die einwirkung des lichtes auf eine alkoholische nitrobenzollösung, Ber. Dtsch. chem, Ges. 19 (1886) 2899–2900, https://doi.org/10.1002/cber.188601902276.
[5] B. König, Photocatalysis in organic synthesis – past, present, and future, Eur. J. Org. Chem. 2017 (2017) 1979–1981, https://doi.org/10.1002/ejoc.201700420.
[6] C.K. Prier, D.A. Rankic, D.W.C. MacMillan, Visible light photoredox catalysis with transition metal complexes: applications in organic synthesis, Chem. Rev. 113 (2013) 5322–5363, https://doi.org/10.1021/cr300503r.
[7] L. Marzo, S.K. Pagire, O. Reiser, B. König, Visible-light photocatalysis: does it make a difference in organic synthesis? Angew. Chem. Int. Ed. 57 (2018) 10034–10072, https://doi.org/10.1002/anie.201709766.
[8] J. Twilton, C. Le, P. Zhang, M.H. Shaw, R.W. Evans, D.W.C. MacMillan, The merger of transition metal and photocatalysis, Nature Rev. Chem. 1 (2017) 0052, https://doi.org/10.1038/s41570-017-0052.
[9] Y. Abderrazak, A. Bhattacharyya, O. Reiser, Visible-light-induced homolysis of earth-abundant metal-substrate complexes: a complementary activation strategy in photoredox catalysis, Angew. Chem. Int. Ed. 60 (2021) 21100–21115, https://doi.org/10.1002/anie.202100270.
[10] P. Herr, C. Kerzig, C.B. Larsen, D. Häussinger, O.S. Wenger, Manganese(I) complexes with metal-to-ligand charge transfer luminescence and photoreactivity, Nat. Chem. 13 (2021) 956–962, https://doi.org/10.1038/s41557-021-00744-9.
[11] K.P.S. Cheung, S. Sarkar, V. Gevorgyan, Visible light-induced transition metal catalysis, Chem. Rev. 122 (2022) 1543–1625, https://doi.org/10.1021/acs.chemrev.1c00403.
[12] S.M. Stevenson, M.P. Shores, E.M. Ferreira, Photooxidizing chromium catalysts for promoting radical cation cycloadditions, Angew. Chem. Int. Ed. 54 (2015) 6506–6510, https://doi.org/10.1002/anie.201501220.
[13] A. Gualandi, M. Marchini, L. Mengozzi, M. Natali, M. Lucarini, P. Ceroni, P.G. Cozzi, Organocatalytic enantioselective alkylation of aldehydes with $[Fe(bpy)_3]Br_2$ catalyst and visible light, ACS Catal. 5 (2015) 5927–5931, https://doi.org/10.1021/acscatal.5b01573.
[14] S. Parisien-Collette, A.C. Hernandez-Perez, S.K. Collins, Photochemical synthesis of carbazoles using an $[Fe(phen)_3](NTf_2)_2/O_2$ catalyst system: catalysis toward sustainability, Org. Lett. 18 (2016) 4994–4997. 10.1021/acs.orglett.6b02456.
[15] C.F. Harris, C.S. Kuehner, J. Bacsa, J.D. Soper, Photoinduced cobalt(III) −trifluoromethyl bond activation enables arene C−H trifluoromethylation, Angew. Chem. Int. Ed. 57 (2018) 1311–1315, https://doi.org/10.1002/anie.201711693.
[16] O. Reiser, Shining light on copper: unique opportunities for visible-light-catalyzed atom transfer radical addition reactions and related processes, Acc. Chem. Res. 49 (2016) 1990–1996. 10.1021/acs.accounts.6b00296.
[17] C. Minozzi, A. Caron, J.-C. Grenier-Petel, J. Santandrea, S.K. Collins, Heteroleptic copper(I)-based complexes for photocatalysis: combinatorial assembly, discovery, and optimization, Angew. Chem. Int. Ed. 57 (2018) 5477–5481, https://doi.org/10.1002/anie.201800144.
[18] K. Rybicka-Jasińska, W. Shan, K. Zawada, K.M. Kadish, D. Gryko, Porphyrins as photoredox catalysts: experimental and theoretical studies, J. Am. Chem. Soc. 138 (2016) 15451–15458, https://doi.org/10.1021/jacs.6b09036.
[19] C.B. Larsen, O.S. Wenger, Photoredox catalysis with metal complexes made from earth-abundant elements, Chem. Eur. J. 24 (2018) 2039–2058, https://doi.org/10.1002/chem.201703602.
[20] Y. Zhang, J.L. Petersen, C. Milsmann, A. Luminescent Zirconium(IV), Complex as a molecular photosensitizer for visible light photoredox catalysis, J. Am. Chem. Soc. 138 (2016) 13115–13118, https://doi.org/10.1021/jacs.6b05934.
[21] B.M. Hockin, C. Li, N. Robertson, E. Zysman-Colman, Photoredox catalysts based on earth-abundant metal complexes, Catal. Sci. Technol. 9 (2019) 889–915, https://doi.org/10.1039/C8CY02336K.
[22] O.S. Wenger, Photoactive complexes with earth-abundant metals, J. Am. Chem. Soc. 140 (2018) 13522–13533, https://doi.org/10.1021/jacs.8b08822.
[23] H. Liu, H. Li, N. Luo, F. Wang, Visible-light-induced oxidative lignin C–C bond cleavage to aldehydes using vanadium catalysts, ACS Catal. 10 (2020) 632–643, https://doi.org/10.1021/acscatal.9b03768.
[24] S. Gazi, W.K. Hung Ng, R. Ganguly, A.M. Putra Moeljadi, H. Hirao, H.S. Soo, Selective photocatalytic C–C bond cleavage under ambient conditions with earth abundant vanadium complexes, Chem. Sci. 6 (2015) 7130–7142, https://doi.org/10.1039/C5SC02923F.
[25] S. Zavahir, Q. Xiao, S. Sarina, J. Zhao, S. Bottle, M. Wellard, J. Jia, L. Jing, Y. Huang, J.P. Blinco, H. Wu, H.Y. Zhu, Selective oxidation of aliphatic alcohols using molecular oxygen at ambient temperature: mixed-valence vanadium oxide photocatalysts, ACS Catal. 6 (2016) 3580–3588, https://doi.org/10.1021/acscatal.6b00753.
[26] R.M. Bullock, J.G. Chen, L. Gagliardi, P.J. Chirik, O.K. Farha, C.H. Hendon, C.W. Jones, J.A. Keith, J. Klosin, S.D. Minteer, R.H. Morris, A.T. Radosevich, T.B. Rauchfuss, N.A. Strotman, A. Vojvodic, T.R. Ward, J.Y. Yang, Y. Surendranath, Using nature's blueprint to expand catalysis with Earth-abundant metals, Science 369 (2020) eabc3183, https://doi.org/10.1126/science.abc3183.
[27] V.R. Pattabiraman, J.W. Bode, Rethinking amide bond synthesis, Nature 480 (2011) 471–479, https://doi.org/10.1038/nature10702.
[28] E. Valeur, M. Bradley, Amide bond formation: beyond the myth of coupling reagents, Chem. Soc. Rev. 38 (2009) 606–631, https://doi.org/10.1039/B701677H.
[29] J.M. Humphrey, A.R. Chamberlin, Chemical synthesis of natural product peptides: coupling methods for the incorporation of noncoded amino acids into peptides, Chem. Rev. 97 (1997) 2243–2266, https://doi.org/10.1021/cr950005s.
[30] F. Albericio, Developments in peptide and amide synthesis, Curr. Opin. Chem. Biol. 8 (2004) 211–221, https://doi.org/10.1016/j.cbpa.2004.03.002.
[31] D. Petzold, M. Giedyk, A. Chatterjee, B. König, A Retrosynthetic Approach for Photocatalysis, Eur. J. Org. Chem. 2020 (2020) 1193–1244, https://doi.org/10.1002/ejoc.201901421.
[32] G.E.M. Crisenza, P. Melchiorre, Chemistry glows green with photoredox catalysis, Nat. Commun. 11 (2020) 803, https://doi.org/10.1038/s41467-019-13887-8.
[33] N. Iqbal, E.J. Cho, Visible-light-mediated synthesis of amides from aldehydes and amines via *in situ* acid chloride formation, J. Org. Chem. 81 (2016) 1905–1911. 10.1021/acs.joc.5b02726.
[34] G. Pandey, S. Koley, R. Talukdar, P.K. Sahani, Cross-dehydrogenating coupling of aldehydes with amines/R-OTBS ethers by visible-light photoredox catalysis: synthesis of amides, esters, and ureas, Org. Lett. 20 (2018) 5861–5865. 10.1021/acs.orglett.8b02537.
[35] L. Xu, S.Z. Zhang, W. Li, Z.H. Zhang, Visible-light-mediated oxidative amidation of aldehydes by using magnetic CdS quantum dots as a photocatalyst, Chem. Eur. J. 27 (2021) 5483–5491, https://doi.org/10.1002/chem.202005138.
[36] L. Wang, M. Yu, C. Wu, N. Deng, C. Wang, X. Yao, Synthesis of Ag/g-C_3N_4 composite as highly efficient visible-light photocatalyst for oxidative amidation of

aromatic aldehydes, Adv. Synth. Catal. 358 (2016) 2631–2641, https://doi.org/10.1002/adsc.201600138.
[37] F.K.C. Leung, J.F. Cui, T.W. Hui, K.K.Y. Kung, M.K. Wong, Photooxidative amidation of aldehydes with amines catalyzed by Rose Bengal, Asian J. Org. Chem. 4 (2015) 533–536, https://doi.org/10.1002/ajoc.201500076.
[38] G.N. Papadopoulos, C.G. Kokotos, One-pot amide bond formation from aldehydes and amines via a photoorganocatalytic activation of aldehydes, J. Org. Chem. 81 (2016) 7023–7028. 10.1021/acs.joc.6b00488.
[39] D. Leow, Phenazinium salt-catalyzed aerobic oxidative amidation of aromatic aldehydes, Org. Lett. 16 (2014) 5812–5815, https://doi.org/10.1021/ol5029354.
[40] X.F. Wang, S.S. Yu, C. Wang, D. Xue, J. Xiao, BODIPY catalyzed amide synthesis promoted by BHT and air under visible light, Org. Biomol. Chem. 14 (2016) 7028–7037, https://doi.org/10.1039/C6OB00736H.
[41] H. Inagawa, S. Uchida, E. Yamaguchi, A. Itoh, Metal-free oxidative amidation of aromatic aldehydes using an anthraquinone-based organophotocatalyst, Asian J. Org. Chem. 8 (2019) 1411–1414, https://doi.org/10.1002/ajoc.201900256.
[42] A. Hassan Tolba, M. Krupička, J. Chudoba, R. Cibulka, Amide bond formation via aerobic photooxidative coupling of aldehydes with amines catalyzed by a riboflavin derivative, Org. Lett. 23 (2021) 6825–6830. 10.1021/acs.orglett.1c02391.
[43] N.F. Nikitas, M.K. Apostolopoulou, E. Skolia, A. Tsoukaki, C.G. Kokotos, Photochemical activation of aromatic aldehydes: synthesis of amides, hydroxamic acids and esters, Chem. Eur. J. 27 (2021) 7915–7922, https://doi.org/10.1002/chem.202100655.
[44] S. Kundu, D. Mondal, K. Bhattacharya, A. Endo, D. Sanna, E. Garribba, M. Chaudhury, Nonoxido vanadium(IV) compounds involving dithiocarbazate-based tridentate ONS ligands: synthesis, electronic and molecular structure, spectroscopic and redox properties, Inorg. Chem. 54 (2015) 6203–6215. 10.1021/acs.inorgchem.5b00359.
[45] K.E. Jolley, M.R. Chapman, A.J. Blacker, A general and atom-efficient continuous-flow approach to prepare amines, amides and imines via reactive N-chloramines, Beilstein J. Org. Chem. 14 (2018) 2220–2228.
[46] A. Porcheddu, L.D. Luca, Iron-catalyzed amidation of aldehydes with N-Chloroamines, Adv. Synth. Catal. 354 (2012) 2949–2953, https://doi.org/10.1002/adsc.201200659.
[47] B. Zhou, J. Du, Y. Yang, Y. Li, Rhodium(III)-catalyzed intermolecular direct amidation of aldehyde C–H bonds with N-chloroamines at room temperature, Org. Lett. 15 (2013) 2934–2937, https://doi.org/10.1021/ol400921r.
[48] N. Alandini, L. Buzzetti, G. Favi, T. Schulte, L. Candish, K.D. Collins, P. Melchiorre, Amide synthesis by nickel/photoredox-catalyzed direct carbamoylation of (Hetero)aryl bromides, Angew. Chem. Int. Ed. 59 (2020) 5248–5253, https://doi.org/10.1002/anie.202000224.
[49] S. Gaspa, A. Valentoni, G. Mulas, A. Porcheddu, L. DeLuca, Metal-free preparation of α-H-chlorinated alkylaromatic hydrocarbons by sunlight, ChemistrySelect 3 (2018) 7991–7995, https://doi.org/10.1002/slct.201801168.
[50] N. Radhoff, A. Studer, Functionalization of α-C(sp3)−H bonds in amides using radical translocating arylating groups, Angew. Chem. Int. Ed. 60 (2021) 3561–3565, https://doi.org/10.1002/anie.202013275.
[51] S. Gaspa, A. Farina, M. Tilocca, A. Porcheddu, L. Pisano, M. Carraro, U. Azzena, L. De Luca, Visible-light photoredox-catalyzed amidation of benzylic alcohols, J. Org. Chem. 85 (2020) 11679–11687, https://doi.org/10.1021/acs.joc.0c01320.
[52] C. Wegeberg, O.S. Wenger, Luminescent first-row transition metal complexes, J. Am. Chem. Soc. Au 1 (2021) 1860–1876, https://doi.org/10.1021/jacsau.1c00353.
[53] L. Dell'Amico, V.M. Fernández-Alvarez, F. Maseras, P. Melchiorre, Light-driven enantioselective organocatalytic β-benzylation of enals, Angew. Chem. Int. Ed. 56 (2017) 3304–3308, https://doi.org/10.1002/anie.201612159.
[54] A. de Aguirre, I. Funes-Ardoiz, F. Maseras, Four oxidation states in a single photoredox nickel-based catalytic cycle: a computational study, Angew. Chem. Int. Ed. 58 (2019) 3898–3902, https://doi.org/10.1002/anie.201814233.
[55] A. de Aguirre, V.M. Fernandez-Alvarez, F. Maseras, A. Lledós, G. Ujaque, Computational modeling of selected photoactivated processes. New Directions in the Modeling of Organometallic Reactions, Springer International Publishing, Cham, 2020, pp. 131–152.
[56] R.H. Li, B. Zhu, S. Wang, Y. Geng, L.K. Yan, Z.M. Su, L.S. Yao, R.L. Zhong, W. Guan, Theoretical mechanistic study of metallaphotoredox catalysis: C–N cross-coupling via Ni(ii)-mediated σ-bond metathesis, Org. Chem. Front. 7 (2020) 2168–2178, https://doi.org/10.1039/D0QO00458H.
[57] J. Xu, Y. Yang, X. Zhao, C. Liu, D. Zhang, DFT mechanistic study of Ir^{III}/Ni^{II}-metallaphotoredox-catalyzed difluoromethylation of aryl bromides, Inorg. Chem. 60 (2021) 8682–8691. 10.1021/acs.inorgchem.1c00645.
[58] M. Yuan, O. Gutierrez, Mechanisms, challenges, and opportunities of dual Ni/photoredox-catalyzed C(sp2)–C(sp3) cross-couplings, WIREs Comput. Mol. Sci. 12 (2022) e1573, https://doi.org/10.1002/wcms.1573.
[59] M.J. Frisch, et al., Gaussian 09, Revision D.01, Gaussian, Inc., Wallingford, CT, 2010.
[60] A.V. Marenich, C.J. Cramer, D.G. Truhlar, Universal Solvation model based on solute electron density and on a continuum model of the solvent defined by the bulk dielectric constant and atomic surface tensions, J. Phys. Chem. B 113 (2009) 6378–6396, https://doi.org/10.1021/jp810292n.
[61] T. Yanai, D.P. Tew, N.C. Handy, A new hybrid exchange–correlation functional using the Coulomb-attenuating method (CAM-B3LYP), Chem. Phys. Lett. 393 (2004) 51–57, https://doi.org/10.1016/j.cplett.2004.06.011.
[62] S. Grimme, J. Antony, S. Ehrlich, H. Krieg, A consistent and accurate ab initio parametrization of density functional dispersion correction (DFT-D) for the 94 elements H-Pu, J. Phys. Chem. 132 (2010) 154104, https://doi.org/10.1063/1.3382344.
[63] M.M. Francl, W.J. Pietro, W.J. Hehre, J.S. Binkley, M.S. Gordon, D.J. DeFrees, J.A. Pople, Self-consistent molecular orbital methods. XXIII. A polarization-type basis set for second-row elements, J. Phys. Chem. 77 (1982) 3654–3665, https://doi.org/10.1063/1.444267.
[64] D. Andrae, U. Häußermann, M. Dolg, H. Stoll, H. Preuß, Energy-adjustedab initio pseudopotentials for the second and third row transition elements, Theor. Chim. Acta 77 (1990) 123–141, https://doi.org/10.1007/BF01114537.
[65] A. Ehlers, M. Böhme, S. Dapprich, A. Gobbi, A. Höllwarth, V. Jonas, K. Köhler, R. Stegmann, A. Veldkamp, G. Frenking, A set of f-polarization functions for pseudo-potential basis sets of the transition metals *Sc*–Cu, Y–Ag and La–Au, Chem. Phys. Lett. 208 (1993) 111–114.
[66] F. Weigend, R. Ahlrichs, Balanced basis sets of split valence, triple zeta valence and quadruple zeta valence quality for H to Rn: design and assessment of accuracy, Phys. Chem. Chem. Phys. 7 (2005) 3297–3305, https://doi.org/10.1039/B508541A.
[67] A. Cabré, G. Sciortino, G. Ujaque, X. Verdaguer, A. Lledós, A. Riera, Iridium-catalyzed isomerization of N-Sulfonyl aziridines to allyl amines, Org. Lett. 20 (2018) 5747–5751. 10.1021/acs.orglett.8b02450.
[68] V.S. Bryantsev, M.S. Diallo, W.A. Goddard III, Calculation of solvation free energies of charged solutes using mixed cluster/continuum models, J. Phys. Chem. B 112 (2008) 9709–9719.
[69] S.I. Gorelsky, AOMix: Program for Molecular Orbital Analysis http://www.sg-chem.net/, version 6.52, 2011,
[70] J.N. Harvey, M. Aschi, H. Schwarz, W. Koch, The singlet and triplet states of phenyl cation. a hybrid approach for locating minimum energy crossing points between non-interacting potential energy surfaces, Theor. Chem. Acc. 99 (1998) 95–99, https://doi.org/10.1007/s002140050309.
[71] F. Neese, Software update: the ORCA program system, version 4.0, Wiley Interdiscip. Rev. Comput. Mol. Sci. 8 (2017) e1327, https://doi.org/10.1002/wcms.81.
[72] G. Sciortino, A. Lledós, P. Vidossich, Bonding rearrangements in organometallic reactions: from orbitals to curly arrows, Dalton Trans 48 (2019) 15740–15752, https://doi.org/10.1039/C9DT03063H.
[73] J.P. Perdew, K. Burke, M. Ernzerhof, Generalized gradient approximation made simple [Phys. Rev. Lett. 77, 3865 (1996)], Phys. Rev. Lett. 78 (1997) 1396-1396.
[74] B.G. Lippert, J.H. Parrinello, Michele, a hybrid Gaussian and plane wave density functional scheme, Mol. Phys. 92 (1997) 477–488, https://doi.org/10.1080/002689797170220.
[75] S. Goedecker, M. Teter, J. Hutter, Separable dual-space Gaussian pseudopotentials, Phys. Rev. B 54 (1996) 1703–1710, https://doi.org/10.1103/PhysRevB.54.1703.
[76] M. Krack, Pseudopotentials for H to Kr optimized for gradient-corrected exchange-correlation functionals, Theor. Chem. Acc. 114 (2005) 145–152, https://doi.org/10.1007/s00214-005-0655-y.
[77] S. Gaspa, I. Raposo, L. Pereira, G. Mulas, P.C. Ricci, A. Porcheddu, L. De Luca, Visible light-induced transformation of aldehydes to esters, carboxylic anhydrides and amides, New J. Chem. 43 (2019) 10711–10715, https://doi.org/10.1039/C9NJ01984G.
[78] S. Gaspa, A. Porcheddu, L. De Luca, Recent developments in oxidative esterification and amidation of aldehydes, Tetrahedron Lett. 57 (2016) 3433–3440, https://doi.org/10.1016/j.tetlet.2016.06.115.
[79] D. Prat, O. Pardigon, H.-.W. Flemming, S. Letestu, V. Ducandas, P. Isnard, E. Guntrum, T. Senac, S. Ruisseau, P. Cruciani, P. Hosek, Sanofi's Solvent Selection Guide: a Step Toward More Sustainable Processes, Org. Process Res. Dev. 17 (2013) 1517–1525, https://doi.org/10.1021/op4002565.
[80] R.K. Henderson, C. Jiménez-González, D.J.C. Constable, S.R. Alston, G.G.A. Inglis, G. Fisher, J. Sherwood, S.P. Binks, A.D. Curzons, Expanding GSK's solvent selection guide – embedding sustainability into solvent selection starting at medicinal chemistry, Green Chem. 13 (2011) 854–862, https://doi.org/10.1039/C0GC00918K.
[81] S.C. Larsen, D.N. Chasteen, R. Hanson Graeme, L. Berliner, Hyperfine and quadrupolar interactions in vanadyl proteins and model complexes: theory and experiment. Metals in Biology. Applications of High-Resolution EPR to Metalloenzymes, Springer Science Business Media, LLC 2010, New York, 2010, pp. 371–409.
[82] N.D. Chasteen, Biological Magnetic Resonance, Plenum Press ed., 1981.
[83] T.S. Smith II, R. LoBrutto, V.L. Pecoraro, Paramagnetic spectroscopy of vanadyl complexes and its applications to biological systems, Coord. Chem. Rev. 228 (2002) 1–18, https://doi.org/10.1016/s0010-8545(01)00437-4.
[84] See the electronic supporting information (ESI) for further details.
[85] L. Eberson, V. Gold, D. Bethell, Electron-transfer reactions in organic chemistry. Advances in Physical Organic Chemistry, Academic Press, 1982, pp. 79–185.
[86] C.J. Ballhausen, H.B. Gray, The electronic structure of the vanadyl ion, Inorg. Chem. 1 (1962) 111–122, https://doi.org/10.1021/ic50001a022.
[87] D. Rehder, Bioinorganic Vanadium Chemistry, John Wiley & Sons, Ltd, Chichester, 2008.
[88] M.B. Smith, J. March, March's Advanced Organic Chemistry, Wiley-VCH Verlag GmbH & Co, 2001.
[89] M. Álvarez-Moreno, C. de Graaf, N. López, F. Maseras, J.M. Poblet, C. Bo, Managing the computational chemistry big data problem: the iochem-BD platform, J. Chem. Inf. Model. 55 (2015) 95–103, https://doi.org/10.1021/ci500593j.